Chapter 2

Experiment and Simulation

2.1 Nuclear Emulsion

In this study we employ the age old nuclear photo-emulsion technique to collect the experimental data. Emulsion experiments involve fixed targets, where the target medium itself acts as the detector. Some excellent reviews and texts [1–3] are available on the details of nuclear emulsion technique. However for the sake of completeness, we summarize here some of the essential features of the nuclear emulsion technique and the data collection method. The first use of photographic emulsion to record charged particle tracks was made in 1891, when α-particles were found to affect silver bromide grains along the paths they traveled [4]. However, during 1940's due to the efforts of various commercial firms like Ilford Ltd. (London), Kodak Ltd. (New York), and to a great extent due to the contribution of the emulsion research group in the University of Bristol (UK), nuclear emulsion technique became an effective and successful tool in cosmic-ray, nuclear and particle physics research. The usefulness of this technique can be understood from its rich history of being a key detector in discovering several new particles like the charged π and K-mesons, the Σ^+ and $\bar{\Lambda}$ baryons, etc. In spite of a stiff competition offered by the modern sophisticated detectors and dedicated electronic readout technology, even in a not so distant past the emulsion experiments have contributed significantly in the field of high-energy hadron-nucleus and nucleus-nucleus (AB) interactions.

Nuclear photographic emulsion is basically a dispersion of silver halide crystals within a gelatin matrix. The medium is used to record charged particle tracks of silver halide micro-crystals embedded into about equal parts in volume, a matrix material comprising mainly of gelatin and water with a small amount of glycerol and a few other substances. An electrically charged particle while passing through the medium, produces latent image along its track that upon proper chemical treatment appears as trails of black colloidal grains of metallic silver along the trajectory of the particle. Compared to an ordinary photographic plate, nuclear emulsion pellicles have several distinguishing features, Nuclear emulsion pellicles are much thicker (thickness ranging between several hundreds to $\sim 10^3$ microns) as compared to only several microns in case of ordinary photographic plates. The photo-sensitive silver halide material (mostly AgBr molecules) has three to four times more concentration in nuclear emulsion than that in a conventional photographic plate. The AgBr grains in nuclear emulsions are well separated and are much smaller in size (less than a micron in diameter), whereas the AgBr grains in an ordinary photographic plate are interlocked and they can be as large as several microns. The Ilford G5 emulsion pellicles are used in this experiment where the grain diameter is about 0.3 micron. However, the mean crystal grain diameters are different in different types of emulsions. It is observed that the contrast of nuclear emulsion may be improved if the grains are uniform in size, and the sensitivity goes up with increasing grain size. The dimension of each Ilford G5 emulsion pellicle used in the present investigation is 18 cm. $\times$ 7 cm. $\times$ 600 microns. Gelatin being a hygroscopic material emulsion can absorb water from the atmosphere. Therefore, while citing the relative composition of emulsions it is necessary to refer to the real time relative humidity of the surroundings. At a relative humidity of 58% each gram of Ilford nuclear emulsion contains about 0.83 gm. of silver halide and 0.162 gm. of gelatine while the corresponding volume ratio is about 45 : 55. The chemical composition of a standard research emulsion (such as Ilford G5) is given in Table 2.1. In emulsion the total number of atoms per c.c. is 7.898×10^{22}, whereas the total number of electrons is 1.0446×10^{24} per c.c. Taking the nuclear radius parameter $r_0 = 1.2$ fm, the geometrical mean free path of all elements in nuclear emulsion comes out to be approximately 37 cm. However, the actual interaction mean free path is quite different from this geometrical value.

2.1.1 Particle Track Formation

When a charged particle passes through nuclear emulsion it losses energy through electromagnetic interaction. The energy lost by the charged particle is transferred to the electrons of the target atoms present in the emulsion medium, and if the transferred energy is greater than the ionization potential of the target atoms, electrons are liberated and the atoms are ionized. As a result silver specks are formed within the silver halide crystal grains. They

Table 2.1: Chemical composition of standard emulsion.

Element	Atomic weight (A)	No. of atoms per cc $\times 10^{20}$	Moles per cc $\times 10^{-3}$	Concentration at 58% R.H.
H	1.008	321.56	53.571	0.074
C	12.0	138.30	22.698	0.227
N	14.01	31.68	5.147	0.053
O	16.0	94.97	16.050	0.007
S	32.06	1.353	0.216	0.249
Br	79.92	100.41	16.673	1.338
Ag	107.88	101.01	16.764	1.817
I	129.93	0.565	0.094	0.012

serve as 'latent images' which when undergo proper chemical treatment become visible. It may be mentioned here that the most important mode of energy loss of a charged particle is the ionization, and it depends on the atomic number and kinetic energy of the incoming particle. In the development process the silver specks act as catalysts for the action of weak reducing agents that deposit additional silver atoms from the same crystal. The deposited silver which appears as black grains under a microscope is permanently embedded into the gelatin through a fixing process. The unexposed silver halide crystals that remain unaffected in the development bath, are removed in the fixing bath. Thus the trail of opaque silver grains form a permanent track structure. To get a good track resolution, the emulsion should have very small grain size and a low density of background grains. It also depends on the emulsion sensitivity and energy of the moving particle as well. Various characteristics of the tracks formed in emulsion are discussed in the next section.

2.1.2 Track Structure

• **Grain Density:** The grain density dn/dx is defined as the number of silver grains deposited per unit (say 100 micron) path length of a track. The grain density is found to be proportional to the rate of energy loss (dE/dx) of the moving particle. However, for high values of dE/dx the proportionality may not always be valid. For an incoming particle of mass m, charge $Z_p e$ and velocity $\beta(= v/c)$ that is large compared to the velocity of the K-shell electrons of the stopping material (in this case emulsion), the average restricted energy loss per unit distance (also called the specific energy loss) is given by [5]

$$-\frac{dE}{dx} = \frac{4\pi Z_p^2 e^4 N Z_t}{mv^2}\left[\ln\left(\frac{2mv^2}{I}\right) - \ln(1-\beta^2) - \beta^2\right], \tag{2.1}$$

where N is the number of atoms per c.c. of emulsion material, Z_t and I are respectively, the mean atomic number and ionization potential of the emulsion nuclei. In terms of dE/dx an empirical expression for the grain density is obtained as [6],

$$\frac{dn}{dx} = \kappa \left[1 - \exp\left\{-bZ_p \left(\frac{dE}{dx}\right)^{\frac{1}{2}} - \sqrt{\alpha}\right\}\right]. \tag{2.2}$$

Here κ and b are experimentally determinable constants that depend on the type of emulsion and the developing material used, and α is the minimum specific energy loss required to ensure that grains are developed. Thus in order to estimate the specific energy loss dE/dx and hence the velocity of the moving charged particles, one can see that the grain density is a useful parameter. It is determined by counting the number of developed grains within a measured length of the track. Sometimes instead of grain density, the blob density B is measured. A blob is a resolvable spot in which more than one grains are present. The estimation of blob number is equivalent to measuring the number of gaps between two blobs. It is observed that the frequency distribution of the gap length follows an exponentially decaying nature [7]. According to [8], the number density of gaps H exceeding a gap length value l is

$$H(l) = B \exp(-g\ l), \tag{2.3}$$

where the slope parameter g is a measure of the grain density, but cannot be set exactly equal to the true grain density dn/dx. Fowler and Perkins gave another relation for the blob density

$$B = g \exp(-g\ \alpha'), \tag{2.4}$$

where α' is a parameter determined by the average developed grain size. From these two relations one can determine g as a useful ionizing parameter.

• **Lacunarity and Opacity:** The lacunarity L of a track is defined as the fraction of a track that is made up of gaps. In terms of the grain density g it is expressed as,

$$L = \int_0^\infty -l \left(\frac{dH}{dl}\right) dl = \exp(-g\ \alpha'). \tag{2.5}$$

From Eq. (2.4) and Eq. (2.5) we get $g = B/L$ and $\alpha' = -(L/B)\ln L$. For particles with low Z and high velocity ($\beta \approx 1$) the specific energy loss is small, and a proportionality like

$$\frac{dE}{dx} \propto \frac{dn}{dx} \tag{2.6}$$

holds. Assuming $g \approx dn/dx$, one may relate Z of the particle with L as, $Z^2 \propto -\ln L$. Opacity O on the other hand, is defined as the fraction of a track that is made up of blobs, and therefore it is related to lacunarity as, $O = 1 - L$. Thus the charge of a particle can be

determined either by measuring its lacunarity or opacity. By default for low charge values ($Z \leqslant 3$) a high degree of accuracy for the charge measurement can be achieved in this method because

$$\delta Z \propto \frac{1}{Z}\,\frac{\delta L}{L}. \tag{2.7}$$

Here the error in L measurement, $\delta L = \sigma_L/\sqrt{N_c}$ can arbitrarily be reduced by increasing N_c, the number of cells of equal length over which the measurement of L has been made. $\sigma_L = \sqrt{< L^2 > - < L >^2}$ is the variance in L.

• **Delta Ray:** For high charge values (usually for $Z \geqslant 4$) the rate of energy loss of the moving particle is high, and secondary electrons are produced with sufficient kinetic energies, and some of these electrons may have observable tracks within emulsion. Such electron tracks are referred to as delta rays. The number of delta rays (n_δ) is also dependent on dE/dx. Therefore, when lacunarity measurement is not possible, the method of delta ray counting can be utilized to determine the charge of a particle. For a particle of charge Ze the number of delta rays with energies between W and $W + dW$ is given as [9],

$$dn_\delta = \frac{2\pi\, N\, Z_p^2\, e^4}{m_e\, v^2}\,\frac{dW}{W}\left[1 - \beta^2\,\frac{W}{W_{\max}}\right]. \tag{2.8}$$

Where m_e is the electron rest mass, and

$$W_{\max} = \frac{2\ m_e\ c^2\beta^2\gamma^2}{1 + 2\gamma\left(\frac{m_e}{m}\right) + \left(\frac{m_e}{m}\right)^2} \tag{2.9}$$

being the upper energy limit that the electron may have received, and $\gamma = \sqrt{1-\beta^2}$ is the Lorentz factor. The lower limit of delta ray energy is found to be more or less 10 KeV. Integrating Eq. (2.8) one obtains, $n_\delta \propto Z^2/\beta^2$. For particles moving with relativistic speed, $\beta \approx 1$ and hence a relation like, $n_\delta \propto Z^2$ can be utilized to determine the charge of such particles.

• **Particle Range:** Charged particles loose energy through collisions with the atoms present in the medium through which they traverse. When the energy of the moving particle becomes less than the ionization potential of the atoms present in the medium, the particle in motion suffers multiple elastic scattering and ultimately stops within the medium. The track length of the particle is the distance along the trajectory starting from its point of origin to the last developed grain. It is also known as the residual range (R). The true range can then be defined as the distance traveled by the particle before it stops within the emulsion. From the knowledge of specific energy loss dE/dx and initial energy E_0, the range of a charged particle can be determined,

$$R(E_0) = \int_0^{E_0} \frac{1}{dE/dx}\ dE. \tag{2.10}$$

Using the expression for dE/dx, the above relation can be written as,

$$R(E_0) = \frac{m}{Z^2}\, f(v_0) \tag{2.11}$$

where v_0 is the initial velocity. In the nonrelativistic limit ($E_0 < m\,c^2$) a range-energy relation for any particle is similar to that of a proton, $R_p = K\,E_p^n$, where R is in microns and the kinetic energy E_p is in MeV. Here K (typical value 0.262) and n (typical value 0.575) are experimentally obtained parameters. For an arbitrary particle of mass m and charge Ze the range-energy relation is derived to be [10]

$$E = K \left(\frac{m}{m_p}\right)^{(1-n)} Z^{2n}\, R^n, \tag{2.12}$$

where m_p is the proton rest mass. Due to different types of uncertainties and fluctuations, range of even mono-energetic particles exhibit straggling. A straggling parameter may be defined as,

$$\Gamma_R = \frac{\pi}{2}\left[\frac{\sum_{i=1}^{N}(R_i - \bar{R})^2}{N}\right]^{1/2}. \tag{2.13}$$

The full width at half maximum (ΔR) of the differential distribution curve of ranges is related to Γ_R as, $\Delta R = 0.94\ \Gamma_R$.

• **Track Width:** For a highly ionizing particle (usually $Z > 10$) the linear track structure contains little information in terms of grain or blob density, and n_δ becomes too large to be counted. Under such circumstances, the track width has been found to be a useful parameter to identify the charge of the particle [3]. The track width depends on various factors such as, the type of emulsion and the developer used, the particle variables like charge, mass, velocity etc. Experimental data show that the track width increases linearly with particle charge for $Z \geqslant 10$. As the track caused by a heavy-ion reaches toward its end, a thinning down (tapering) of the track is observed due to electron capture, which reduces the effective charge of the ion. The length of this tapered portion (L_t) of the track may also be used to find out the atomic number of the particle [11]. An empirical relation like $L_t = C\,Z^\nu$ with $\nu \approx 1$ has been obtained in this connection.

• **Shrinkage Factor:** Since gelatin is a hygroscopic material, the actual equilibrium thickness and index of refraction of both the processed and unprocessed emulsion depend on the surrounding humidity. Consequently, we define the shrinkage factor (S) as,

$$S = \frac{\text{thickness of emulsion plate during exposure}}{\text{thickness of emulsion plate during scanning}}. \tag{2.14}$$

Thus for any quantitative measurement of the track densities in emulsion, the original thickness of the emulsion has to be known.

2.2 The Microscopy

• **Counting and Statistics:** In an emulsion experiment counting is as important as measurement. Tracks belonging to different categories (to be discussed later) should be properly counted, and the target nucleus should be identified accordingly. The ionization of a track may be measured by counting the number of grains or blobs over a particular track length (say 100 micron). To identify the charge of the particle the delta rays over a similar length interval may also be counted. Energy spectra are determined by counting the number of tracks within particular range intervals. Angular distributions are determined by counting the number of tracks in prescribed angular intervals. Therefore, a practical knowledge of counting statistics is essential in order to justify the reliability of the collected data. The Poisson distribution is usually used for this purpose.

• **Dip Angle:** The dip angle (δ) of a linear track segment is given by

$$\tan\delta = \frac{S\Delta z}{L_{xy}}, \tag{2.15}$$

where Δz is the difference in depth between any two points on the track segment under consideration, L_{xy} is the length of the track projected between these two points on the horizontal (x, y) plane, and S is the shrinkage factor. It has been implicitly assumed that the refractive index of the oil employed for oil immersion objective is very close to the refractive index of the developed emulsion and the glass plate. If dry objectives are used, the apparent depth d_a will be less than the true depth $d_{\rm true}$, which is measured as, $d_{\rm true} = \mu_e d_a$. Here μ_e is the refractive index of the emulsion.

• **Space Angle:** The space angle also known as the emission angle (θ) between two tracks may be measured by the simple co-ordinate method. If the direction cosines of the tracks are (l_1, m_1, n_1) and (l_2, m_2, n_2), then θ is given by

$$\cos\theta = l_1\, l_2 + m_1\, m_2 + n_1\, n_2. \tag{2.16}$$

The direction cosines of a track can easily be obtained by taking space coordinates of any two points on the track. If (x_1, y_1, z_1) and (x_2, y_2, z_2) are the space points on the track, the direction cosines are given as

$$(l, m, n) \equiv \left(\frac{x_1 - x_2}{d}, \frac{y_1 - y_2}{d}, \frac{z_1 - z_2}{d}\right) \tag{2.17}$$

with $d = \left[(x_1 - x_2)^2 + (y_1 - y_2)^2 + (z_1 - z_2)^2\right]^{1/2}$. The azimuthal plane is defined as a plane perpendicular to the direction of motion of the incoming projectile nucleus. The track direction projected onto the azimuthal plane with respect to some reference direction may

be defined as the azimuthal angle (φ) of the track. If the projectile direction is taken as one of the displacement directions (say x-direction), then the azimuthal angle is given by,

$$\varphi = \tan^{-1}\left(\frac{S\ \Delta z}{\Delta y}\right). \tag{2.18}$$

If the projectile direction does not completely coincide with the specified x-direction, then φ for a particular track may be measured by setting the corresponding quantity for the projectile track as zero. The track geometry is schematically presented in Fig. 2.1. Due to scattering the track of a charged particle in emulsion may not always be straight. Therefore, it is convenient to break up the track into M number of essentially straight segments, and the residual range of the particle may be determined from the relation,

$$R = \sum_{i=1}^{M}\left[(x_i - x_{i-1})^2 + (y_i - y_{i-1})^2 + S^2(z_i - z_{i-1})^2\right]^{1/2}. \tag{2.19}$$

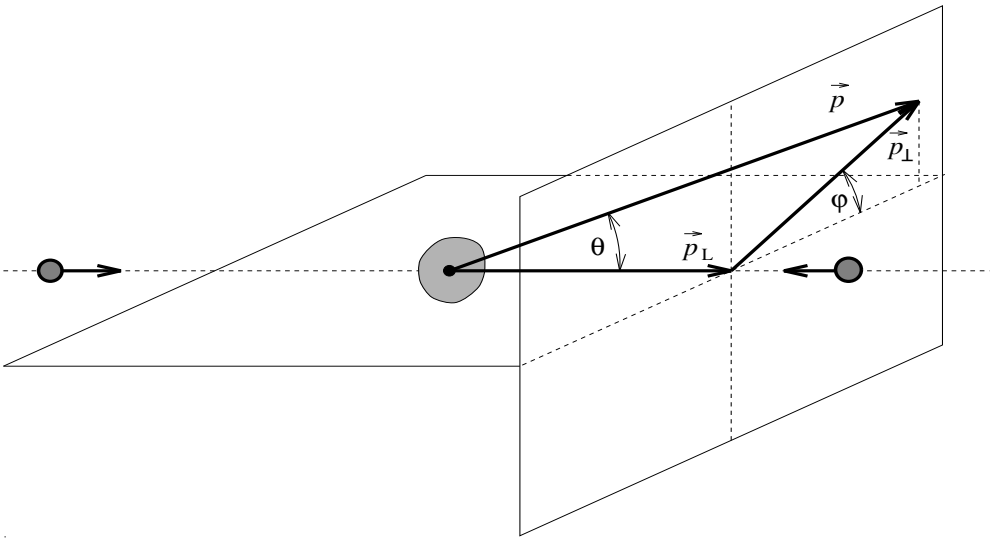

Figure 2.1: Schematic of a secondary track geometry with respect to the projectile.

• **Momentum Measurement:** While passing through emulsion medium, charged particles experience frequent small deflections due to elastic scattering with the Coulomb field of the atomic nuclei present in the medium. The probability for such a deflection having small angular deviations but at high frequency, is governed by Rutherford's scattering formula. A general expression for the projected absolute angle of deviation (ϕ) is theoretically derived by Goudsmit and Sauderson [12] and its mean is given by

$$\bar{\phi} = \frac{\chi\ Z}{p\beta}\left(\frac{t}{100}\right)^{1/2}. \tag{2.20}$$

Where χ is a constant of scattering, defined as

$$\chi = Z_p\, e^2\, Z_t\, N^{1/2} \left[\ln \left(\frac{\phi_{\max}}{\phi_{\min}} \right) \right]^{1/2}. \tag{2.21}$$

Here N is the number of atoms per unit volume in emulsion, Z_t is the average atomic number of the atoms presents in the medium, Z_p is the atomic number of the particle moving with velocity β and p being its momentum, $\phi_{\max}$ ($\phi_{\min}$) is the maximum (minimum) value of the projected angle in the plane of the initial particle trajectory, and t is the path length in the scattering medium. It is necessary to determine the value of $\bar{\phi}$ very accurately in order to find out $p\beta$ value of a track. This can be done following a method suggested by Fowler [8]. In Fowler's method the plate is placed on the mechanical stage of the microscope in such a way that the track is (at least approximately) parallel to one of the sides of the stage, say x-axis. The coordinate (x_0, y_0) of an arbitrary point on the track are measured. The plate is then displaced by a distance equal to the cell length t along x-direction, and the ordinate y_1 of the point is determined by means of an eyepiece scale. The measurement should be performed under a very high magnification (e.g., 2500×), and the ordinate eyepiece scale is commonly replaced by a flair micrometer, which is capable of reading distances within a few hundreds of micron. Once again the stage is moved through the standard distance t, and the ordinate y_2 is recorded. The operation is repeated several times along the length of the track. The absolute value of the second differences taken irrespective of the sign: $D_k = \mid y_{k+2} - 2y_{k+1} + y_k \mid$ of successive such measurements are determined. The mean absolute value between successive chords of length t corrected for stage noise and cell length $\bar{D} = \sum_k^n (D_k/n)$ gives a measure of the scattering parameter through

$$\bar{\phi} = \frac{\bar{D}}{t}\,(180/\pi). \tag{2.22}$$

From the above relation $p\beta$ (in MeV/c) can be evaluated. In a given cell length t of the track, the energy loss must be negligible if $\bar{\phi}$ is to be a meaningful quantity.

2.2.1 Scanning Emulsion Plates

In a scanning process events (or interactions, also called stars) of a certain types are located in a systematic way. In area (more specifically volume) scanning the focal surface is continually shifted to sweep up and down from the surface of the emulsion to the supporting glass. This is done by rolling the fine focus control while observing the events successively coming into and going out of view. Each field of view is scanned throughout its depth from one surface of the emulsion to the other. For high efficiency the field may be divided into a number of sufficiently small separate areas, so that the entire volume can be covered as

the traverse is made. Generally area scanning is performed under either of the following two circumstances, (i) when events of a certain type within a given volume of emulsion are to be found, and (ii) if the situation demands a representative sample of events. Preliminary volume or line scanning may be performed under a magnification of $300 - 400\times$, but the angle measurement and track identification process may finally be done under a total magnification of $1500\times$. It would be worthwhile to note that volume scanning is not an effective method for finding out single diffractive dissociation events and/or interactions with H-nuclei. Only high multiplicity events easily catch human eyes. Therefore, to get an unbiased sample of events area/volume scanning is not recommended. For that purpose the technique of along the track scanning is preferred. In this technique each projectile track is carefully followed from the leading edge of a plate along its length until the projectile interacts or leaves the plate. Like the area scanning, the preliminary scanning along the track may be performed under $300 - 400\times$ total magnification, though the final selection of events has to be done under a higher magnifications (say at $1500\times$). There can be no denial that the emulsion scanning is a tiresome and time consuming process, and it requires a lot of patience and concentration on the part of a scanner. Accuracy of an emulsion experiment depends largely on the skill of the observer. To avoid individual bias counter checking of the same data sample by independent observers is therefore, recommended. By adopting along the track scanning method in emulsion experiments it is possible to build up a sample of minimum bias events.

2.3 Data Characteristics

Stacks of Ilford G5 nuclear photographic emulsion pellicles of size 18 cm $\times$ 7 cm $\times$ 600 μm, were horizontally irradiated to a beam of ^{28}Si nuclei at an incident energy of 14.5A GeV (Experiment No. E847) from the Alternating Gradient Synchrotron (AGS) at the Brookhaven National Laboratory (BNL) [13]. The flux of incident ^{28}Si nuclei was 3×10^3 ions per square centimeter. The equivalent nucleon-nucleon (NN) center of mass energy $\sqrt{s_{NN}} = 5.382$ GeV. If the AB collision is considered as a superposition of many incoherent NN collisions, then for a central collision where all 28 nucleons of the ^{28}Si nucleus participate in the interaction, this amounts to a total center of mass energy $\sqrt{s} \approx 151$ GeV. On the other hand, if the AB interaction is considered as a coherent collision between an incoming ^{28}Si nucleus and a stationary Ag or Br nucleus (for which the weighted average mass number $A \approx 94$), then the total center of mass energy comes out to be $\sqrt{s} \approx 275$ GeV. These are two extreme limits, and the actual center of mass energy is perhaps somewhere in between the two extreme cases mentioned. However, the above quoted values of $\sqrt{s}$ give a qualitative idea about the center of mass energy scale of the interactions, and not to determine the exact

degree of coherence. To find out the primary ^{28}Si-emulsion stars Leitz microscopes with a total magnification of 300× were utilized, and the emulsion plates were scanned along individual projectile tracks. According to the emulsion terminology, tracks emitted from a star are classified into four categories namely, the shower tracks, the gray tracks, the black tracks, and the projectile fragments.

• **Shower Tracks:** The shower tracks are caused by singly charged particles moving with relativistic speed ($\beta > 0.7$). This category comprises of particles produced in a high energy interaction, most of which are charged pi-mesons. The ionization of a shower track $I \leqslant 1.4\, I_0$, where I_0 ($\approx$ 20 grains/100 microns) is the minimum ionization due to any track observed within a G5 plate. The total number of such tracks in an event is denoted by n_s.

• **Gray Tracks:** The gray tracks are generally due to the protons that have directly participated in an interaction and are knocked out from the target nuclei. They usually fall within an energy range of 30 – 400 MeV. The ionization limit of gray tracks is $1.4\, I_0 < I \leqslant 6.8\, I_0$ and its range is $\geqslant$ 3 mm in standard emulsion. A few percent of the gray tracks may also be due to the slow moving mesons. The velocity range of these particles is $0.3c$ to $0.7c$. The number of gray tracks in an event is denoted by n_g.

• **Black Tracks:** Black tracks are predominantly originate from the slowly moving protons and other heavier fragments emitted by the excited target nucleus after an interaction has taken place. Their velocity is $< 0.3c$, and for a black track caused by a proton the kinetic energy $<$ 30 MeV. Ionization of these category of particles is greater than $6.8\, I_0$, and range less than 3 mm. in emulsion. The number of black tracks in an event is denoted by n_b.

• **Projectile Fragments:** The projectile fragments are the spectator parts of the incident nucleus that do not directly participate in an interaction. Having almost same energy and/or momentum per nucleon as the incident projectile, these fragments exhibit uniform ionization over a long range and suffer negligible scattering. Their number in an event is denoted by n_{pf}. The projectile fragments are emitted within an extremely narrow forward cone along the beam direction whose semi-vertex angle θ_F is decided by the momentum of the incoming nucleus ($p_{\rm inc}$). For a given $p_{\rm inc}$ and Fermi momentum ($p_{_F}$) of the target nucleus, θ_F is defined as,

$$\theta_F = p_F/p_{\rm inc}. \tag{2.23}$$

According to a simple Fermi gas model the Fermi energy of a nucleus is given by

$$E_F = \frac{\hbar^2}{2m_N}\left(\frac{3}{2}\pi^2 n_N\right)^{2/3}, \tag{2.24}$$

where m_N and n_N are, respectively, the nucleon mass and nucleon number density. The Fermi momentum is calculated from E_F through: $p_F = \sqrt{2m_N E_F}$. Roughly, p_F is estimated

to be 200 MeV/c for the silicon nucleus. For a projectile nucleus having 14.5A GeV of kinetic energy, $\theta_F \approx 0.013$ rad. In an event n_{pf} denotes the number of projectile fragments of charge $z \geqslant 2$ falling within this cone.

• **Event Selection:** A sample of inelastic events can be classified into two different categories namely, the electromagnetic dissociation (ED) events and the nuclear events. Extremely strong electromagnetic fields offered by the target nuclei causes electromagnetic dissociation of the projectile nuclei. The ED events typically consist only of projectile fragments [14]. Barring the ED events, rest of the events in the sample may be considered as nuclear interactions. Nuclear interactions are subdivided into peripheral (large impact factor) and central (small impact factor) collisions in terms of their shower multiplicities. The target of an interaction, whether a light nucleus (H, C, N, O) or a heavy nucleus (Ag, Br), is decided by the number of heavy tracks (n_h) produced from the event. The total number of heavy tracks of an event is $n_h = n_b + n_g$. By imposing a restriction $n_h \geqslant 8$ with at least one fragment of charge $Z \geqslant 2$ per event, it can be ensured that the interaction is either with an Ag nucleus or with a Br nucleus. An event with $n_h < 8$ can either be an Ag/Br or a light nucleus (H, C, N, O) event. A further restriction on the number of spectator projectile fragments in an event n_{pf} $(Z \geqslant 2) = 0$ enable us to choose only those interactions where total fragmentation of the incident ^{28}Si nucleus has taken place. By following 113.25 mts. of primary track length a total of 1003 events were found, which is equivalent to a mean free path of $\lambda_{tot} = 11.29 \pm 0.36$ cms. for ^{28}Si nuclei in emulsion and which corresponds to a total cross section $\sigma_{tot} = 1121 \pm 34$ mb. Among 1003 primary events, 88 events were due to the ED of the ^{28}Si projectile and the rest were due to inelastic interactions. The experimental value of the mean free path for the latter class of events is $\lambda_{inel} = 12.38 \pm 0.41$ cm., and the corresponding cross-section $\sigma_{inel} = 1023 \pm 34$ mb [13]. From a simple geometric participant-spectator model [15], the AB interaction cross-section is given as

$$\sigma_{th} = \pi r_0^2 \left[A_p^{1/3} + A_t^{1/3} - \delta \right]^2 , \tag{2.25}$$

where A_t (A_p) is the target (projectile) mass number. In our case $A_p = 28$, and the weighted average target mass number of emulsion nuclei (Table 2.1) is taken to be $A_t = 29.10$. This gives $\sigma_{th} = 1262.02$ mb, where $r_0 = 1.2$ fm. and $\delta = 0.83$ have been used. In Fig. 2.2 we have shown a plot of reaction cross-section in the framework of the participant-spectator model [16]. Due to intrinsic inefficiency associated with human bias, in particular to detect diffractive dissociation and electromagnetic dissociation events, the present experimental value of σ_{tot} is slightly lower than the universal trend.

After counting measurements are completed, the emission angle (θ) with respect to the

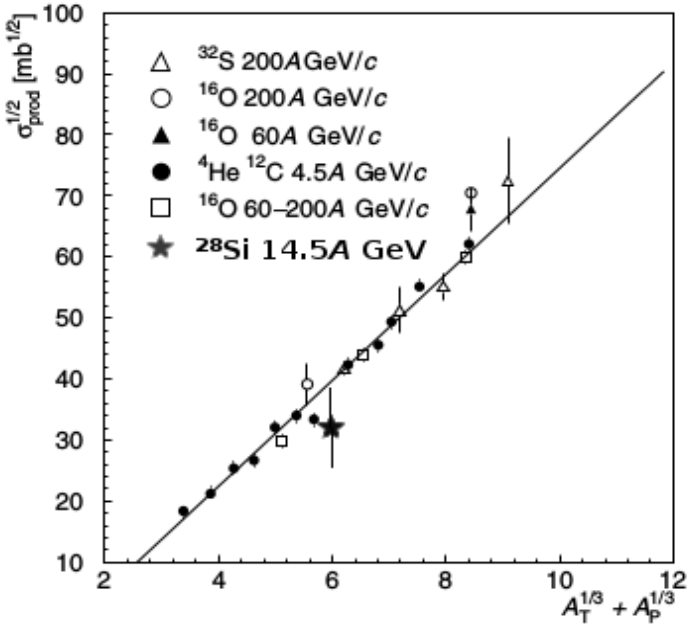

Figure 2.2: Plot of reaction cross-section with $A_p^{1/3} + A_t^{1/3}$ up to SPS energy

projectile nucleus and the azimuthal angle (φ) of each track were measured. The angle measurement are performed by using 100× oil immersion objectives at a total magnification of 1500× with the help of Koristka microscopes. In an emulsion experiment the pseudorapidity (η) together with the azimuthal angle (φ) of a track constitutes a convenient pair of basic variables in terms of which the particle emission data can be analyzed. Knowing θ, the η variable can be determined. As mentioned in Section 1.2, when energy and/or momentum measurements are difficult as it is the case for emulsion experiment, and where in comparison with the total energy the rest mass of a particle can be neglected, as it is the case for most of the charged mesons produced in high energy interactions, the pseudorapidity variable is a convenient replacement of the rapidity variable. The η-resolution is given as

$$\delta\eta = -\frac{1}{\sin\theta}\delta\theta. \tag{2.26}$$

So, at small angles only a small error in θ measurement can ensure a good resolution in η. An accuracy of $\delta\eta = 0.1$ unit of pseudorapidity and $\delta\varphi = 1$ mrad. could be achieved through the reference primary method of angle measurement. Following the criteria mentioned above a sample of ^{28}Si-Ag/Br events of size $N_{ev} = 331$ is considered for further analysis. Our analysis is confined only to the shower tracks having an average shower track multiplicity $\langle n_s \rangle = 52.67 \pm 1.33$. To avoid contamination between the singly charged produced particles and the spectator projectile protons, shower tracks falling within the Fermi cone were excluded from our analysis. Distribution of both η and φ for all the shower tracks in the event sample

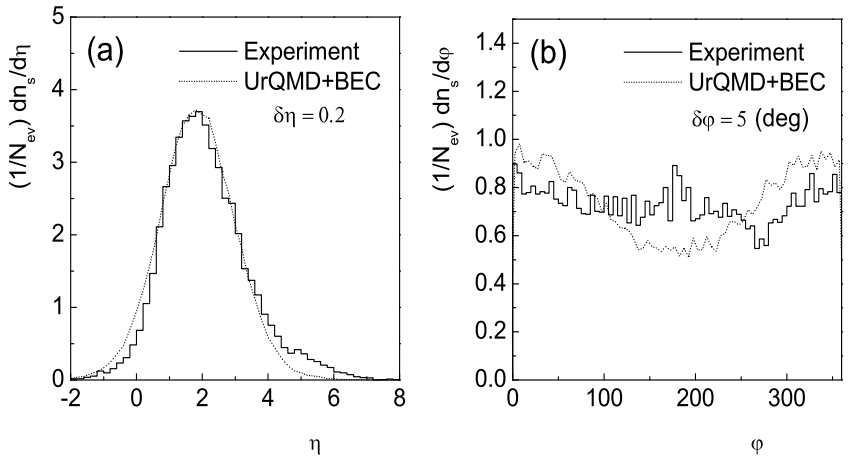

Figure 2.3: Distributions of (a) pseudorapidity and (b) azimuthal angle of shower tracks emitted from ^{28}Si-Ag/Br interaction at 14.5A GeV.

have been obtained in terms of the respective density functions

$$\rho(x) = \frac{1}{N_{ev}} \frac{dn_s}{dx}, \tag{2.27}$$

with $x = \eta$ or φ. The η-distribution of shower tracks can be approximated by a Gaussian function like,

$$\rho(\eta)d\eta = \rho_0 \exp\left[-\frac{(\eta - \eta_0)^2}{2\sigma_\eta^2}\right] d\eta, \tag{2.28}$$

where ρ_0 is the peak density, η_0 is the centroid and σ_η is the width of the distribution. The experimental η and φ-distributions are shown in Fig. 2.3. The η-distribution is fitted to Eq. (2.28). The fit parameters are, $\rho_0 = 17.88$, $\eta_0 = 1.90$ and $\sigma_\eta = 2.17$. The φ-distribution on the other hand, is asymmetric within its accessible range $(0,\ 2\pi)$. The dips in the φ-distribution near $\varphi \approx 90^0$ and 270^0 may either be due to inefficient recording of shower tracks in the directions vertical to the emulsion plane, exactly toward or away from the direction of vision, or it may be due to a dynamical reason like azimuthal asymmetry (flow), or it may be due to the combination of both.

The energy density in the central η region can be estimated by making use of Bjorken's formula (1.72). While applying the formula two important points have to be kept in mind: (i) that the production of neutral pions in any high energy interaction is as abundant as either of their charge varieties, and (ii) that the overlapping area ($\mathcal{A}$) between the projectile (^{28}Si nucleus) and target Ag (or Br) is almost equal to the geometrical area of a ^{28}Si nucleus. Therefore, the factor $dN/dy \approx dN/d\eta$ in Bjorken's formula has to be replaced by 1.5 $dn_s/d\eta$. Note that dN/dy is the rapidity density of all produced particles in the given sample. Keeping these two factors in mind and putting $\langle m_t \rangle = \sqrt{m^2 + \langle p_t \rangle^2} \approx 0.38$ GeV and $\tau_0 = 1$ fm/c, we obtain $\epsilon \approx 1.5$ GeV/fm^3 for a subsample of events with shower track multiplicity $n_s \geqslant 50$. Note that even for the subsample with a high number of produced particles, the

energy density value is just above the threshold required for the onset of a QGP like state, which according to the lattice QCD is approximately a few GeV/fm^3 [17]. In soft processes like multiparticle production, it is even more difficult to extract the signature of such a state, even if it is formed. Therefore, though we do not aspire to conclusively establish a QGP formation in the present colliding system, obviously the multiparticle production phenomenon, which itself is an interesting topic in heavy-ion collision, can be statistically analyzed. Based on the Glauber model following a method prescribed in [18], for a subsample of events falling within a limited shower multiplicity range, one can even obtain a rough estimate of the collision centrality and hence the average impact parameter ($\bar{b}$), from the number density of shower tracks in the central η region. In this method the peak value of the η density of produced charged particles in AB collision at an impact parameter b is related to the same density for pp interaction at the same energy by the following relation:

$$\frac{dN_{ch}}{d\eta}(b)\Big|_{AB} \approx 1.28\frac{AB}{A^{2/3}+B^{2/3}}\ \frac{1}{1+a(A^{1/3}+B^{1/3})}\ \exp\left(-b^2/2\beta^2\right)\ \frac{dN_{ch}}{d\eta}\,|_{pp}\ . \quad (2.29)$$

Here a is a parameter obtained by linear fitting of $dN_{ch}/d\eta$ against $A^{1/3}$ for different AB collisions at 14.5A GeV. For our event sample with $n_s \geqslant 50$ we obtained $\bar{b} = 4.45$ fm.

2.4 Merits and Demerits of Emulsion Experiments

One of the main advantages of nuclear emulsion is that, it can be used as a detector of charged particles as well as a target medium comprising of nuclei of varying mass numbers. As mentioned above, standard emulsions consist of H, C, N, O, Ag and Br nuclei. As far as high-energy interactions are concerned, information regarding target nucleus mass can be obtained from the characteristic appearances of an event. Nuclear emulsion has the ability to detect all charged particles coming out of an event (also called a star) i.e., emulsion as a detector has 4π acceptance. However, the detection efficiency is not equally good in all directions. Particularly along the vertical direction (along the thickness of the plates) the efficiency is not very good. The stopping power of nuclear emulsion is usually very high due to its high medium density, and therefore, the interaction probability between a projectile particle and a target nucleus is also very large. This in other words means an ultra-high energy particle that may easily pass through any other detector even without interacting, has a very small possibility to pass through an emulsion plate without creating any track. As a detector nuclear emulsion is less costly, light weight and very easy to handle. The sensitivity of undeveloped nuclear emulsion pellicle lasts for a few weeks. Hence all charged particles passing through it are able to get their tracks permanently recorded within a long span of time. That makes emulsion a suitable detector for balloon flight and satellite experiments to

study the cosmic-ray events where the projectile / beam is rarely found. In nuclear emulsion neutral particles can also be indirectly detected, as and when they interact with the light nuclei, particularly Hydrogen, and produce tracks of charged particles. The same mechanism is used in the scintillation detectors to detect neutral particles, specially neutrons. Nuclear emulsion can be used from the temperature of liquid Helium up to the boiling point of water. The most striking advantage of nuclear emulsion is its high spatial resolution. For conventional horizontally irradiated stacks of emulsion pellicles, in spite of multiple Coulomb scattering and distortion effects, an accuracy of 0.1 unit of pseudorapidity can be achieved. This unique feature makes the emulsion experiments important to investigate distributions of produced particles in narrow intervals of pseudorapidity space.

There are some difficulties associated with the emulsion experiments too. It is not possible to identify the sign of a charged particle unless a magnetic field is applied. But it is difficult to get the magnetic field penetrate into the emulsion material, hence to produce enough curvature in the track of a relativistic particle to identify its charge. The sensitivity and thickness of emulsion pellicles are affected by temperature, humidity, age etc. Unless special care is taken these factor always introduce some error in the data. The track lengths of most of the produced particles in emulsion are at best a few millimeter long. So high magnification devices such as high power microscopes are required to scan and collect data. Moreover, till date no automated device could be designed for scanning emulsion pellicles, so we totally depend on our eyes. This makes the data acquisition process a tedious and time consuming process. For AB interactions at GeV energy range, where a few hundreds of particles may come out of an event, the time taken to build up even a moderate statistics requires huge effort. The collected data can never be fully free from personal bias and errors. However, such errors can be reduced through counter checking by more than one independent observer. Identification of target fragments often becomes extremely difficult, and sometimes even impossible. Therefore, in the data collection process it is often impossible to exactly identify the target nucleus of the interaction. However, as mentioned in Section 2.3 a gross distinction between the light group (H, C, N, O) and the heavy group (Ag, Br) of target nuclei can be made.

2.5 The Simulation

We know that a complete theoretical description of high-energy AB collisions requires exact QCD calculations. But due to the intrinsic complexities associated with the QCD, non-perturbative effects are treated through model calculations. In our analysis we use the the Ultra-relativistic Quantum Molecular Dynamics (UrQMD) [19] model to simulate the experiment in most of the cases. However, on one occasion (Ring-jet analysis, Chapter 6) we have

also used the RQMD model [20]. Both RQMD and UrQMD are transport models where an AB interaction is considered as a superposition of many elementary NN interactions, and simulates the entire history of the space-time evolution an AB event, starting from its initial pre-equilibrium stage to the final freeze-out. Brief descriptions of both the models are given in Section 1.5. While a provision to accommodate nuclear emulsion as a probable target has been made in the RQMD model, the same in UrQMD cannot be automatically done. The sampling of Ag/Br events generated by UrQMD is described below. Here we describe the salient features of the UrQMD model in details.

The UrQMD model is a microscopic model based on a phase space description of nuclear reactions. It describes the phenomenology of hadronic interactions at low and intermediate energies ($\sqrt{s} < 5$ GeV) in terms of interactions between known hadrons and their resonances. At higher energies ($\sqrt{s} > 5$) GeV, the excitation of color strings and their subsequent fragmentation into hadrons are taken into account. The model was proposed mainly for a microscopic description of AB interactions. Note that up to now there is no unique theoretical description of the underlying hadron-hadron interactions, with their vastly different characteristics at different incident energies and in different kinematic intervals. Perturbative quantum chromodynamics (pQCD) can be applied to describe hard processes, processes with large four-momentum (Q^2) transfer. But pQCD is formally inappropriate for the description of soft processes because of the small Q^2 values. Therefore, low-p_t collisions are described in terms of phenomenological models. With advance computation facilities available now-a-days a vast variety of models for hadronic and nuclear collisions can be implemented. The UrQMD model is one of them which is quite appropriate for the collision energy involved in the present experiment.

The UrQMD model is based on the covariant propagation of all hadrons considered on the (quasi)particle level on classical trajectories in combination with stochastic binary scatterings, color string formation and resonance decay. It represents a Monte Carlo solution of a large set of coupled partial integro-differential equations for the time evolution of the various phase space densities of particle species $i = N, \Delta, \Lambda, \pi$, etc. The main ingredients of the model are the cross sections of binary reactions, the two-body potentials and the decay widths of resonances. Projectile and target are modeled according to a Fermi-gas ansatz. The nucleon are represented by a Gaussian shaped density distribution,

$$\varphi_j(\boldsymbol{x}_j, t) = \left(\frac{2\alpha}{\pi}\right)^{3/4} \exp\left[-\alpha\{(\boldsymbol{x}_j - r_j(t)\}^2 + \frac{i}{\hbar}\boldsymbol{p}_j(t)\boldsymbol{x}_j\right]. \tag{2.30}$$

The wave function of the nucleus is defined as the product of single nucleon Gaussian functions without invoking the Slater determinant that is necessary for antisymmetrization.

Therefore, the total N-body wave function is given as

$$\Phi = \prod_i \varphi_i(\boldsymbol{x}_j, \boldsymbol{p}_j, t). \tag{2.31}$$

In configuration space the centroids of the Gaussian are distributed at random within a sphere of radius

$$R(A) = r_0 \left(\frac{1}{2} \left[A + (A^{1/3} - 1)^3 \right] \right)^{1/3} : \quad r_0 = \left(\frac{3}{4\pi\rho_0} \right)^{1/3}, \tag{2.32}$$

where ρ_0 is the nuclear matter density in the ground state. The finite widths of these Gaussians result in a diffused surface region beyond the radius of that sphere. The initial momenta of the nucleons are randomly chosen between 0 and the local Thomas-Fermi momentum,

$$p_F^{\max} = \hbar c \ \left(3\pi^2\rho\right)^{\frac{1}{3}}, \tag{2.33}$$

ρ is the corresponding local nucleon density. A disadvantage of the initialization mentioned above is that the initialized nuclei are not really in their ground state with respect to the Hamiltonian used for their propagation. However, the parameters of the Hamiltonian are tuned to the equation of state of finite nuclear matter and to properties of finite nuclei, e.g., binding energy, root mean square radius, etc. If however, the energy of the nucleons within the nucleus is minimized according to the Hamiltonian in a self consistent fashion, then the nucleus would collapse to a single point in momentum space because the Pauli principle has not been taken into account in the Hamiltonian. One possible solution to this problem is the inclusion of fermionic properties of the nucleons via the anisymmetrization of the wave function of the nucleus. This ansatz has been implemented in the framework of the Fermionic Molecular Dynamics (FMD) [21]. But the FMD equations of motion are computationally very expensive. To get rid of the problems one can use the so called Pauli potential [22] in the Hamiltonian. Its advantage is that the initialized nuclei remain absolutely stable, whereas in the conventional initialization and propagation without the Pauli potential, the nuclei start evaporating single nucleons after approximately 20–30 fm/c. A drawback of the potential is that the kinetic momenta of the nucleons are not anymore equivalent to their canonical momenta, i.e. the nucleons carry the correct Fermi-momentum, but their velocities are zero. Furthermore, the Pauli potential leads to a wrong specific heat and changes the dynamics of fragment formation.

For AB collisions the interaction potential used in UrQMD is the density dependent Skyrme potential. This potential consists of a sum of two and a three-body interaction term. The two-body term (E^{Sk2}) having a linear density dependence, models the long-range attractive component of the NN interaction, whereas the three-body term (E^{Sk3}) with its quadratic

density dependence is responsible for the short-range repulsive part of the interaction. In addition to the Skyrme potential, Yukawa (E^{Yuk}), Coulomb (E^{Coul}) and Pauli (E^{Pauli}) (optional) potentials are also implemented in the UrQMD model. In finite nuclei the usage of a Yukawa term has the advantage that the parameter can be tuned to the proper surface potential of the nuclei without changing the equation of state. Currently only CASCADE mode or a hard Skyrme equation of state are available in the UrQMD. The default mode is CASCADE, the hard Skyrme equation of state is limited to incident beam energies below 4.0 GeV per nucleon. With these interactions the classical UrQMD Hamiltonian can be written as,

$$\mathcal{H} = \sum_{j=1}^{N} E_j^{\mathrm{kin}} + \frac{1}{2}\sum_{j,k=1}^{N}\left(E_{jk}^{\mathrm{Sk2}} + E_{jk}^{\mathrm{Yuk}} + E_{jk}^{\mathrm{Coul}} + E_{jk}^{\mathrm{Pauli}}\right) + \frac{1}{6}\sum_{j,k,l=1}^{N} E_{jkl}^{\mathrm{Sk3}}. \tag{2.34}$$

The equation of motion of the many-body system is calculated by means of a generalized variational principle. The time evolution of the system is obtained by the requirement that the action is stationary under the allowed variation of the wave function. This yields an Euler-Lagrange equation for each parameter:

$$\dot{\boldsymbol{p}}_i = -\frac{\partial \langle \mathcal{H} \rangle}{\partial \boldsymbol{q}_i} = -\nabla_{\boldsymbol{q}_i} \sum_{j\neq i} \langle V_{ij} \rangle = -\nabla_{\boldsymbol{q}_i} \langle \mathcal{H} \rangle \tag{2.35a}$$

$$\dot{\boldsymbol{q}}_i = -\frac{\partial \langle \mathcal{H} \rangle}{\partial \boldsymbol{p}_i} = \frac{\boldsymbol{p}_i}{m} + \nabla_{\boldsymbol{p}_i} \sum_{j} \langle V_{ij} \rangle = -\nabla_{\boldsymbol{p}_i} \langle \mathcal{H} \rangle \,, \tag{2.35b}$$

$$\langle V_{ij} \rangle = \int d^3x_1 d^3x_2 \; \varphi_i^* \varphi_j^* \; V(x_1, x_2) \; \varphi_i \varphi_j. \tag{2.35c}$$

These are the time evolution equations which are solved numerically. The equations have the same structure as the classical Hamilton equations. Impact parameter of a collision is sampled according to the quadratic measure, $dW \sim b \; db$. Two particles collide if their relative distance d fulfills the relation, $d \leqslant d_0 = \sqrt{\sigma_{tot}/\pi}$. In UrQMD the total cross section σ_{tot} depends on the center of mass energy $\sqrt{s}$, the particle type and its isospin. The neutron-neutron cross section is set equal to the proton-proton cross section (i.e., isospin-symmetry). In the high-energy limit ($\sqrt{s} \geqslant 5$ GeV) the CERN/HERA parametrization for the proton-proton cross section is used [23]. Since the functional dependence of σ_{tot} on $\sqrt{s}$ at low energies shows a complicated shape, UrQMD uses a table-lookup for those cross sections. For momenta $p_{lab} < 5$ GeV/c, UrQMD uses the following parametrization to obtain a good fit to the data,

$$\sigma_{tot}(p) = \begin{cases} 75.0 + 34.1p^{-1} + 2.6p^{-2} - 3.9p & \text{for} \quad 0.3 < p < 5 \\ 271.6\exp(-1.1p^2) & \text{for} \quad p < 0.3. \end{cases} \tag{2.36}$$

Particle production in UrQMD either takes place via the decay of a meson or baryon resonance or via a string excitation and fragmentation. Up to incident beam energies of 8-10 GeV/nucleon particle production is dominated by resonance decays. Production cross sections for the excitation of individual resonances can be calculated in the framework of the one-pion exchange (OPE) or one-boson exchange (OBE) models [24]. Regarding the number of implemented resonances in UrQMD and considering the limited applicable energy range for cross sections calculated within OPE and OBE models, the calculation of all implemented resonance excitation cross sections in the framework of these models is not practical. Therefore, an effective parametrization based on simple phase space considerations has been employed in UrQMD, and free parameters are tuned to experimental measurements. After the fragmentation, decay of the resonances proceeds according to the branching ratios compiled by the Particle Data Group [23]. The resonance decay products have isotropic distributions in the rest frame of the resonance. If a resonance is among the outgoing particles, its mass must first be determined according to a Breit-Wigner mass distribution. If the resonance decays into $N > 2$ particles, then the corresponding N-body phase space is used to calculate their N momenta stochastically. The Pauli principle is applied to hadronic collisions or decays by blocking the final state, if the outgoing phase space is occupied. The collision term in the UrQMD model includes more than fifty baryon species (including nucleon, delta and hyperon resonances with masses up to 2.25 GeV) and five meson nonets (including strange meson resonances), which are supplemented by their corresponding anti-particles and all isospin-projected states. The states can either be produced in string decays, s-channel collisions or resonance decays. For excitations with higher masses e.g., more than 2 GeV, a string picture is used. Full baryon/antibaryon symmetry is included. Therefore the number of implemented baryons defines the number of antibaryons in the model and the antibaryon-antibaryon interaction is defined via the baryon-baryon interaction cross sections. The framework allows to bridge within one concise model, the entire available range of energies, from the Bevalac region ($\sqrt{s_{NN}} \sim$ a few GeV) to the RHIC ($\sqrt{s_{NN}} = 200$ GeV).

2.5.1 Modeling Bose-Einstein Correlation

The Bose-Einstein correlation (or equivalently, the Hanbury-Brown–Twiss effect) is one of the primary reasons of particle correlation in relativistic nuclear collisions. Even though the phenomena in nuclear and particle physics was introduced more than thirty tears ago, several basic questions concerning the form of the correlation function remain unanswered. With the modernization of computational facility, the level of sophistication both in the theoretical description and in the experimental studies has increased very much, in particular in the field of heavy-ion physics [25]. The Bose-Einstein correlation (BEC) between identical

particles is a quantum statistical effect which is usually not embedded in a classical Monte-Carlo model like the UrQMD model. We know that intensity correlations appear due to the symmetrization of the two-particle states. Suppose that a pair of particles is observed with respective momenta q_1 and q_2. If final state interactions can be neglected, the amplitude of such a final state is proportional to

$$\mathcal{A} \propto \frac{1}{\sqrt{2}} \left[e^{i(q_1 x_1 + q_2 x_2)} + e^{i(q_1 x_2 + q_2 x_1)} \right], \tag{2.37}$$

where x_i $(i = 1,\ 2)$ is the emission point of the i-th particle. If the particles are emitted incoherently, the observed two-particle spectrum is given by

$$\rho_2(q_1, q_2) \propto \int dx_1 \rho_1(x_1) \int dx_2 \rho_1(x_2) |\mathcal{A}(q_1, q_2)|^2, \tag{2.38}$$

and the two-particle intensity correlation function is defined as,

$$D_2(q_1, q_2) = \frac{\rho_2(q_1, q_2)}{\rho_1(q_1)\rho_1(q_2)} = 1 + |d_1(q_1 - q_2)|^2. \tag{2.39}$$

This function carries information about the Fourier-transformed space-time distribution of the particle emission:

$$d_1(q) = d_1(q_1 - q_2) = \int dx e^{iqx} d_1(x) \tag{2.40}$$

as a function of the relative momentum q. As compared to the unsymmetrized case, BECs modify the momentum distribution of the pair of particles in the final state by a weight factor:

$$f_{BEC}(q, x) = \langle 1 + \cos[(q_1 - q_2) \cdot (x_1 - x_2)] \rangle \,. \tag{2.41}$$

A large amount of data exists on the two-particle correlation function. It has been seen that like-charge particle correlations are much stronger than those between unlike-charge particles [26]. These mens that the two and many-particle correlations are mainly due to the Bose-Einstein interference.

Since the model code (UrQMD) employed here to simulate the interactions is a classical Monte-Carlo model, and hence the quantum statistical effects like the Bose-Einstein correlation (BEC) between identical bosons are not embedded into the code. We make an attempt to include the BEC effect numerically in the form of the so called 'after burner' algorithm [27] by making use of the output of the event generator. The particle information are contained in the UrQMD output file '`test.f19`' which is written in accordance with the OSCAR format. Only the (even-wise) pi-mesons are chosen from the output file. Each particle entry in an event contains a serial number, the particle ID, the particle 4-momentum (p_x, p_y, p_z, E), the particle mass m, and the final freeze-out 4-coordinates (x, y, z, t). The

algorithm of the procedure is as follows:

(i) Randomly choose a meson from an event, call it the ith one, and assign a charge *'sign'* i.e., +, − or 0 to it, irrespective of its original charge with weight factors respectively, given by $p_+ = n_+/n$, $p_- = n_-/n$ and $p_0 = n_0/n$. Here n_+, n_-, n_0 are respectively, the number of +ve, −ve and neutral mesons in the event, and $n\,(= n_+ + n_- + n_0)$ is obviously the total number of mesons in that event. This meson, say the ith one, defines a new phase space cell.

(ii) Calculate the distances in the 4-momenta $\delta_{ij}(p) = |p_i - p_j|$ and 4-coordinates $\delta_{ij}(x) = |x_i - x_j|$ between the already chosen meson (i.e., the ith one) and all other mesons (indexed by j) that are not yet assigned any charge *'sign'*.

(iii) Assign a weight factor

$$P_{ij} = \exp\left[-\frac{1}{2}\,\delta_{ij}^2(x)\;\delta_{ij}^2(p)\right] \tag{2.42}$$

to each j-th particle. The weight factor actually characterizes the bunching probability of the particles in a given cell.

(iv) Then start generating uniformly distributed random numbers $r \in (0, +1)$. If $r < P_{ij}$, reassign to the j-th meson the same charge *'sign'* as the i-th one. Continue the process until either r exceeds P_{ij}, or until all mesons in the event having the same charge *'sign'* as the i-th one are exhausted.

(v) Repeat the whole set of operations for all other mesons for which the charge reassignment has not yet been done. Obviously, the weight factors $p_{\pm,0}$ will now be modified, as some of the particles present in the event are already used up. The algorithm is repeated until mesons belonging to all charge varieties in the event are used up.

The UrQMD model provides all pion pairs with $-Q = (p_i - p_j)^2 = (\Delta E)^2 - (\Delta p)^2 < 0$. In order to keep the value of the factor (2.42) below unity, only the pion pairs having space-like separation: $-R^2 = (x_i - x_j)^2 = (\Delta t)^2 - (\Delta x)^2 < 0$ are accepted [28]. Without changing the overall set of 4-momenta, 4-coordinates, or total meson charge of the system, we can in this way generate clusters of identical charge states of mesons. A schematic of such clustering is illustrated in Fig. 2.4.

2.5.2 Sampling ^{28}Si-Ag/Br Simulated Events

Two sets of minimum bias ^{28}Si + Ag and ^{28}Si + Br events at $E_{\rm lab} = 14.5$A GeV are generated separately using UrQMD (the UrQMD input parameter `CToption(27) = 1`). In order to

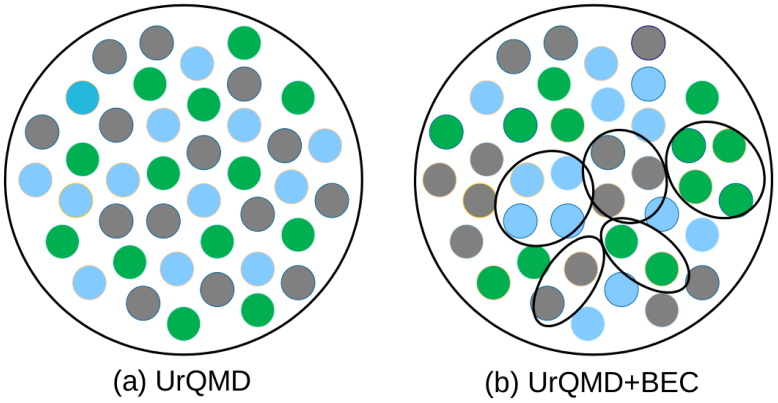

Figure 2.4: An illustration of the effect of the Bose-Einstein correlation algorithm. The phase space distribution of pi-mesons produced in the event generator (UrQMD) is modified by the after burner algorithm of BEC (UrQMD+BEC). Three color varieties represent the members of the pion family.

accommodate the Bose-Einstein correlation into UrQMD, the output files of UrQMD are supplemented by the algorithm mentioned in Section 2.5.1. After that only charged mesons have been retained for subsequent analyses. The event samples corresponding to different target nuclei are then mixed up to produce a new (say) 'hybrid' sample. While doing so, the proportional abundance of Ag and Br nuclei in G5 emulsion is maintained [3]. From the hybrid samples we select events in such a way as to match the experimental s-particle multiplicity distributions. The simulated sample is five times as large as the experimental one. Since the simulated event sample possesses identical multiplicity distribution, the average charged meson multiplicity $\langle n_{ch} \rangle$ is obviously same as the experimental $\langle n_s \rangle$. The η and φ distributions for the simulated sample are overlaid onto their respective experimental distribution, shown in Fig. 2.3. One can see that the simulated event sample possesses more or less similar η-distribution as the experiment. The peak density, centroid and the width of the best Gaussian fit to the simulated η-distribution are also very close to their respective experimental values. The values obtained here are: $\rho_0 = 18.18$, $\eta_0 = 1.80$ and $\sigma_\eta = 2.22$. The φ distribution on the other hand possesses a dip at around 180^0. This once again is due to a preferential emission of charged secondaries in the direction of the reaction plane, or equivalently due to an 'elliptic flow' ($v_2 > 0$) in UrQMD [29].

For error calculation we have generated event samples based on random numbers, where a pair of random numbers representing the η and φ values has been associated with each track. For the pseudorapidity variables we have generated a set of random numbers following Gaussian distribution with the mean and variance as extracted from the experimental sample, and for the azimuthal angle another set of uniformly distributed random numbers with

appropriate limits are generated. The generated sample also possesses identical multiplicity distribution, same η-distribution (actually the best Gaussian fitted distribution) as the experimental sample and uniform φ-distribution. An inverse of integral method is used to generate the Gaussian distributed random numbers, whereas the linear congruential method is used to generate the uniformly distributed random numbers [30]. While generating the random numbers, no correlation has been assumed, and hence these data sets correspond to independent emission of particles. The random number generated sample size is five times larger than the experimental one.

Bibliography

[1] A. Beiser, *Rev. Mod. Phys.* **24**, 273 (1952).

[2] C. F. Powell, P. H. Fowler and D. H. Perkins, *The study of elementary particles by photographic method* (Pergamon, Oxford, 1959).

[3] W. H. Barkas, *Nuclear research emulsions Vol. I and II* (Academic Press, NY, 1963).

[4] M. Reingamum, *Z, Physik* **12**, 1076 (1911).

[5] M. S. Livingstone and H. A. Bethe, *Rev. Mod. Phys.* **9**, 245 (1937).

[6] M. Balu, *Phys. Rev.* **75**, 279 (1949).

[7] C. O'Ceallaigh, *Nuov. Cim. Suppl.* **12**, 412 (1954).

[8] P. H. Fowler and D. H. Perkins, *Phil. Mag.* **46**, 587 (1955).

[9] N. F. Mott, *Proc. Roy. Soc.* (London) **124**, 425 (1929).

[10] C. M. G. Lattes *et al., Proc. Roy. Soc.* (London) **61**, 173 (1948).

[11] P. Freier, E. J. Lofgren, E. P. Ney and F. Oppenheimer, *Phys. Rev.* **74**, 1818 (1948).

[12] S. Goudsmit and J. L. Saunderson, *Phys. Rev.* **58**, 36 (1940).

[13] G. Singh, A. Z. M. Ismail and P. L. Jain, *Phys. Rev.* **C 43**, 2417 (1991).

[14] G. Singh, K. Sengupta and P. L. Jain, *Phys. Rev.* **C 41**, 999 (1990).

[15] G. D. Westfall *et al., Phys. Rev.* **C 19**, 1309 (1979).

[16] J. Letessier and J. Rafelski, *Hadrons and Quark-Gluon Plasma*, (Cambridge University Press, Cambridge, UK, 2004).

[17] F. Karsch, *Nucl. Phys.* **A 698**, 199c (2002).

[18] C. Y. Wong, *Introduction to High-Energy Heavy-Ion Collisions* (World Scientific, 1994).

[19] S. A. Bass *et al., Prog. Nucl. Part. Phys.* **41**, 255 (1998);
M. Bleicher *et al., J. Phys.* **G 25**, 1859 (1999).

[20] H. Sorge, *Phys. Rev.* **C 52**, 3291 (1995);
H. Sorge, H. Stocker and W. Greiner, *Ann. Phys.* **192**, 266 (1989).

[21] H. Feldmeier, *Nucl. Phys.* **A 515**, 147 (1990).

[22] L. Wilets *et al., Nucl. Phys.* **A 282**, 341 (1977).

[23] R. Barnett *et al., Phys. Rev.* **D 54**, 1 (1996).

[24] M. Berenguer, *Thesis*, Goethe University, Frankfurt am Main, Germany (1993).

[25] W. A. Zajc, *Nucl. Phys.* **A 525**, 315c (1991).

[26] A. D. Angelis, *Mod. Phys. Lett.* **A 5**, 2395 (1990).

[27] O. V. Utyuzh, G. Wilk and Z. Wlodarczyk, *Phys. Lett.* **B 522**, 273 (2001).

[28] M. Bystersky, *Nucleonica Supplement* **49**, s37 (2004).

[29] P. P.Bhaduri and S. Chattopadhyay, *Phys. Rev.* **C 81**, 034906 (2010);
Md. Nasim *et al., Phys. Rev.* **C 83**, 054902 (2011).

[30] P. R. Bevington and D. K. Robinson, *Data Reduction and Error Analysis for Physical Sciences* (McGraw-Hill, New York, 2003).